

# Origin of Long Lived Coherences in Light-Harvesting Complexes

Niklas Christensson<sup>1</sup>, Harald F. Kauffmann<sup>1,2</sup>, Tõnu Pullerits<sup>3</sup>, and Tomáš Mančal<sup>4</sup>

<sup>1</sup>*Faculty of Physics, University of Vienna, Strudlhofgasse 4, 1090 Vienna, Austria*

<sup>2</sup>*Faculty of Physics, Vienna University of Technology, 1040 Vienna, Austria*

<sup>3</sup>*Department of Chemical Physics, Lund University, P.O. Box 124, SE-22100 Lund, Sweden and*

<sup>4</sup>*Institute of Physics, Faculty of Mathematics and Physics,*

*Charles University, Ke Karlovu 5, Prague 121 16, Czech Republic*

A vibronic exciton model is developed to investigate the origin of long lived coherences in light-harvesting complexes. Using experimentally determined parameters and uncorrelated site energy fluctuations, the model predicts oscillations in the nonlinear spectra of the Fenna-Matthews-Olson (FMO) complex with a dephasing time of 1.3 ps at 77 K. These oscillations correspond to the coherent superposition of vibronic exciton states with dominant contributions from vibrational excitations on the same pigment. Purely electronic coherences are found to decay on a 200 fs timescale.

The role of quantum mechanics in biological processes, as well as photosynthetic light-harvesting, has been of interest for a long time [1–3]. The topic received renewed attention after the observation of long lived oscillations in the two-dimensional (2D) spectra of the Fenna-Matthews-Olson (FMO) protein pigment complex [4]. These oscillations were interpreted as a signature of electronic coherences between the delocalized energy eigenstates of the complex, and it was argued that their slow dephasing could enhance the efficiency of energy transfer between the chlorosome antenna and the reaction center [4, 5]. Subsequent studies revealed that the oscillations in FMO have a dephasing time of 1.2 ps at 77 K [6], and that such oscillations are a common feature in light-harvesting complexes [7, 8]. Based on the known structure of FMO (Fig. 1), simulations employing formally exact equations of motions for the reduced density operator found oscillations with dephasing times of 200–300 fs - clearly shorter than the experimental observation [5, 9–11]. Significantly longer dephasing times were found if the transition frequency fluctuations (static or dynamic) of the different pigments are assumed to be correlated [12, 13]. However, theoretical studies using molecular dynamics simulations of the interaction between electronic and nuclear degrees of freedom (DOF) have not been able to confirm the existence of such correlations [14], or long lived electronic coherences [15]. To what extent the long lived oscillations in the experiments reflect electronic coherences, or if they influence the transport of energy across the complex [4, 16], thus remains an open question.

Analysis of excitation dynamics in molecular aggregates typically employs a reduced description, where the electronic DOF and their mutual couplings are treated explicitly, and the nuclear modes of the pigments and protein are treated as a heat bath [17, 18]. The presence of underdamped vibrational modes in the bath produces oscillatory signatures in 2D spectra which are similar to the modulations predicted for electronic coherences [19]. The dephasing time of such nuclear coherence are of the order of several picoseconds, and they can often be treated as completely undamped on the time scale of a typical 2D experiment. Low temperature fluorescence line narrowing (FLN) experiments on FMO have

revealed a large number of vibrational modes in the range of 0–350 cm<sup>-1</sup> [20]. However, the oscillations seen in the 2D spectra of FMO cannot be directly related to simple nuclear wavepackets, because the frequency of the oscillations does not match any of the vibrational frequencies, and the Huang-Rhys factors of the modes are too low. On the other hand, recent simulations have revealed unexpected effects on the electronic structure and dynamics if vibrational modes are explicitly included in the system [21]. Motivated by these results, we develop a vibronic exciton Hamiltonian in so called one particle approximation [22, 23] for FMO, in which one vibrational mode on each monomer is treated explicitly. We will show below that this model predicts oscillations in the 2D spectra of FMO with 1.3 ps dephasing times at 77 K, and that these long lived coherences can be traced to superpositions of vibronic exciton states located on the same pigment.

The total Hamiltonian of a molecular aggregate in contact with the environment is partitioned in a standard way into system, bath and system-bath interaction terms,  $H = H_S + H_B + H_{SB}$ . The system Hamiltonian describes the  $Q_y$  transition on each bacteriochlorophyll (BChl) in FMO (see Fig. 1) with the vibrational progression of a single vibrational mode. Including the resonance coupling between the transitions, the system Hamiltonian reads

$$H_S = \sum_{n,\nu,m,\nu'} [\delta_{nm} \delta_{\nu\nu'} (E_n + \nu \hbar \omega_0) + J_{n,\nu;m,\nu'}] |n, \nu\rangle \langle m, \nu'|, \quad (1)$$

where  $E_n$  is the transition frequency of pigment  $n$  (site energy),  $\omega_0$  is the vibrational frequency, and  $\nu$  is the quantum number of the vibrational mode. The coupling energy  $J_{n,\nu;m,\nu'}$  between the individual transitions can be expressed via the electronic resonance coupling  $J_{nm}$  [18] and the Franck-Condon amplitudes of the vibrational mode [23]  $J_{n,\nu;m,\nu'} = \langle \nu | 0 \rangle \langle \nu' | 0 \rangle$ . The eigenvalues and wave-functions of  $H_S$  are given by  $\hbar \omega_\alpha$  and  $|\alpha\rangle = \sum_{n,\nu} c_{n,\nu}^\alpha |n, \nu\rangle$ , respectively. The bath Hamiltonian,  $H_B$ , is described as a collection of independent harmonic oscillators, for which the system-bath interaction is given by  $H_{SB} = \sum_{n,\nu} \omega d_n(\omega) \tilde{q}_n |n, \nu\rangle \langle n, \nu|$ . Here  $\tilde{q}$  is a generalized coordinate of the environment, and  $d(\omega)$

is the displacement of the excited state relative to the ground state. We assume that the system-bath Hamiltonian does not depend on the state of the vibrational mode ( $\nu$ ), implying that a vibrational coherence on an isolated monomer is undamped. Assuming equal but uncorrelated system-bath interaction for the different pigments, the energy gap correlation function in the local basis is given by  $C_{nm}(t) = \omega^2 d_n d_m \langle \tilde{q}_n(t) \tilde{q}_m(0) \rangle = C_0(t) \delta_{nm}$ . When the interaction of the system with the environmental modes (i.e. all except those treated explicitly in the system Hamiltonian) is weak, it is advantageous to perform calculations in the eigenstate basis of the system Hamiltonian. The correlation function of the energy gap in the eigenstate representation can be expressed via the expansion coefficients,  $c_{n,\nu}^\alpha$ , and the correlation function of each excitation in the local basis  $C_0(t)$ ,

$$C_{\alpha\beta}(t) = C_0(t) \left\{ \sum_{n,\nu} (c_{n,\nu}^\alpha)^2 (c_{n,\nu}^\beta)^2 + \sum_{n,\nu \neq \nu'} [(c_{n,\nu}^\alpha)^2 (c_{n,\nu'}^\beta)^2 + (c_{n,\nu'}^\alpha)^2 (c_{n,\nu}^\beta)^2] \right\} = C_0(t) \gamma_{\alpha\beta} \quad (2)$$

The dephasing dynamics of a coherent superposition between the eigenstates  $\alpha$  and  $\beta$  is determined by the line-shape function  $g_{\alpha\beta}(t) = \int_0^t d\tau \int_0^\tau d\tau' \gamma_{\alpha\beta} C_0(\tau')$ . The correlation function  $C_0(t)$  is connected to the spectral density  $\tilde{C}''(\omega)$  via a Fourier transform (see e.g. Ref. [24]). In addition to dephasing, the system-bath interaction leads to relaxation between the eigenstates of the system. We use Redfield theory [17] (Markov and secular approximation), where the relaxation rate is given by

$$k_{\alpha \rightarrow \beta} = 2\pi \sum_{n,\nu,m,\nu'} \delta_{nm} c_{n,\nu}^\alpha c_{m,\nu'}^\alpha c_{n,\nu}^\beta c_{m,\nu'}^\beta \times \left\{ (1 + n(\omega_{\alpha\beta})) \tilde{C}''(\omega_{\alpha\beta}) + n(-\omega_{\alpha\beta}) \tilde{C}''(-\omega_{\alpha\beta}) \right\}, \quad (3)$$

where  $\tilde{C}''(\omega_{\alpha\beta}) > 0$  and  $n(\omega_{\alpha\beta})$  is the Bose-Einstein distribution function. The total relaxation rate from a level  $\alpha$ ,  $\Gamma_\alpha = \frac{1}{2} \sum_{\gamma \neq \alpha} k_{\alpha \rightarrow \gamma}$ , determines the lifetime broadening of this exciton state. Assuming  $k_B T < \hbar \omega_0$ , the linear absorption spectrum can be calculated as [18]

$$OD(\omega) \propto \omega \left\langle \sum_{\alpha} |\mu_{\alpha 0}|^2 \text{Re} \int_0^{\infty} dt e^{-g_{\alpha\alpha}(t) - \Gamma_\alpha t - i(\omega_{\alpha 0} - \omega)t} \right\rangle_{\Delta, \Omega}, \quad (4)$$

where  $\alpha$  runs over all exciton levels and the transition dipole moments  $\mu_{\alpha 0}$  are given by  $\mu_{\alpha 0} = \sum_{n,\nu} c_{n,\nu}^\alpha \mu_n \langle \nu | 0 \rangle$ . Here  $\langle \dots \rangle_{\Delta, \Omega}$  denotes the average over a random distribution of pigment energies and orientations of complexes.

To simulate the oscillations in a third order experiment (i.e. 2D spectra) we adopt the doorway window representation [25]. Of all Liouville pathways contributing to the signal, only those involving a coherence between two levels in the excited state will give rise to oscillations during the waiting time  $t_2$ . Without the loss of generality, we focus on the non-rephasing coherence pathways illustrated in Fig. 1, which give rise to oscillations along

the diagonal in the non-rephasing 2D spectrum [7]. The response function for this pathway is given by

$$R_{\alpha\beta,0} = \langle \langle (\mu_{\alpha 0})^2 (\mu_{\beta 0})^2 \rangle_{\Omega} G_\alpha(t_3) G_{\alpha\beta}^{(2)}(t_2) G_\alpha(t_1) \rangle_{\Delta}, \quad (5)$$

where  $G_\alpha(t) = e^{-i\omega_{\alpha 0} t - \Gamma_\alpha t - g_{\alpha\alpha}(t)}$ , and  $G_{\alpha\beta}^{(2)}(t_2) = e^{-i\omega_{\alpha\beta} t_2 - g_{\alpha\alpha}(t_2) - g_{\beta\beta}(t_2) + 2g_{\alpha\beta}(t_2) - (\Gamma_\alpha + \Gamma_\beta) t_2}$ . In this work we use the site energies ( $E_n$ ) and resonance couplings ( $J_{nm}$ ) for FMO *Chlorobium tepidum* from Ref. [18], and the analytical formula for the overdamped part of the spectral density,  $\tilde{C}''(\omega)$ , extracted from a FLN experiment [20]. The direction of the transition dipole moments were taken from the protein data bank file 3ENI [26]. FLN experiments have identified 30 vibrational modes in FMO, and the strongest feature in the spectrum arises from three modes around 185  $\text{cm}^{-1}$  [20]. To retain a simple description, we treat this cluster of modes as one effective mode with a frequency of  $\omega_0 = 185 \text{ cm}^{-1}$  and a Huang-Rhys factor of 0.05. For calculations with the exciton model, the vibrational mode was included as an underdamped contribution in the spectral density. In all calculations presented in this paper, we sampled the pigment transition energies from a Gaussian distribution with a FWHM of 80  $\text{cm}^{-1}$ .

The vibronic exciton and exciton model predict very similar linear optical properties as illustrated by the simulated linear absorption spectra shown in Fig. 1. Figure 2(a) shows the time evolution of coherences involving the lowest state of the exciton model. During  $t_2$  the signals oscillate with frequencies corresponding to the splitting between the exciton levels and are completely damped after 400 fs. The strong damping can be readily understood from Eqs. (3) and (5). For the exciton model we find that the cross-correlation term  $g_{\alpha\beta}$  is small and the coherence pathways decay mainly with  $\exp(-g_{\alpha\alpha}(t_2) - g_{\beta\beta}(t_2))$ . If a (static or dynamic) correlation of the transition frequency fluctuations in the site basis is assumed (ad hoc), the cross-correlation functions in the exciton basis become larger and enable longer dephasing times.

The coherence pathways involving the lowest levels of the vibronic exciton model are shown in Fig. 2(b). The vibronic exciton coherences are remarkably long lived, and the signals show only minor damping on a 2 ps timescale. The long dephasing time of the coherences in the vibronic exciton model can be understood by inspection of the expansion factors  $\langle |c_{n,\nu}^\alpha|^2 \rangle_{\Delta}$  given in Tab. I and the transition frequency distributions shown in Fig. 1. For instance, state 1 corresponds to 75 % to an excitation of the  $\nu = 0$  transition of pigment 3, while state 4 has a large contribution of vibrational excitation ( $\nu = 1$ ) on the same pigment. As discussed above, the system-bath interaction is independent of the state of the vibrational mode, and these two vibronic exciton levels will therefore experience highly correlated fluctuations, resulting in slow dephasing of the 1, 4 coherence. Despite the large contribution from the vibrational excitation to state 4, it has a transition dipole moment which is comparable to that of the other vibronic exciton levels. For non-

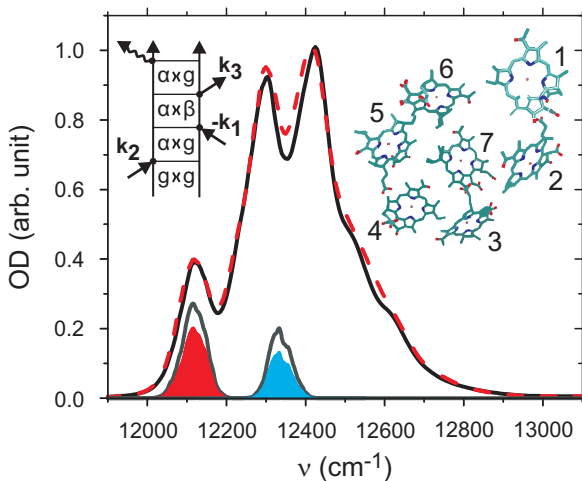


Figure 1: Linear absorption spectrum at 77 K for the exciton model (black) and the vibronic exciton model (red dash). The gray lines show the distribution of renormalized transition frequencies weighted by the transition strength (scaled by 2/3) for state 1 and 4 in the vibronic exciton model. The filled areas illustrate the relative contribution from electronic (red) and vibronic (blue) excitations on pigment 3. The spectra of the vibronic exciton model have been shifted by the reorganization energy of the vibrational mode ( $-9.25 \text{ cm}^{-1}$ ) for comparison. The insets show the Feynman diagram illustrating the non-rephasing excited state coherence pathway in Eq. (12), and the arrangement of the 7 BChls in FMO (*C. tepidum*) [26]. This figure was generated using the VMD software [27].

interacting pigments, only the zero-phonon state ( $\nu = 0$ ) has a significant transition dipole moment. The strong transition dipole moment here is the result of intensity borrowing from the electronic transitions on the other pigments. As illustrated in Fig. 1, state 4 of the vibronic exciton model exhibits both properties needed for the generation of long lived coherences: a large contribution of vibrational excitation of pigment 3, and a strong transition dipole moment enabled by intensity borrowing. The combination of both effects leads to long lived oscillations on the red edge of the linear absorption spectrum as shown in Fig. 2(c). The oscillations show a bi-phasic behavior, where the initial 200 fs decay of the oscillation is due to the decay of coherences between vibronic exciton states localized on different pigments (like the 1, 2 coherence, see Fig. 2(b) and Tab. I), while the long lived oscillations reflect coherences between vibronic exciton states localized on the same pigment. A fit to the oscillations give a dephasing time of 1.3 ps. By comparing to the stimulated emission signal calculated for the same spectral range, we estimate the modulation of the total signal, including stimulated emission and ground state bleach, to be 5 – 10 % for  $t_2 > 0.3 \text{ ps}$ .

The Fourier transform of the signal in Fig. 2(c) is shown in Fig. 2(d). The oscillation frequency of  $205 \text{ cm}^{-1}$  is higher than  $\omega_0$  and also higher than the frequency observed in the experiment ( $160 \text{ cm}^{-1}$ ) [6]. The

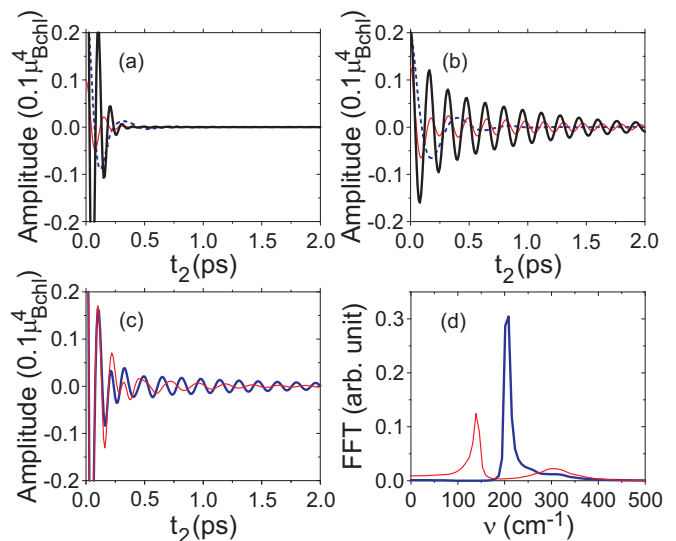


Figure 2: Amplitude of the real part of the non-rephasing coherence pathways involving the lowest state. a)  $Re\langle R_{1\beta}\rangle_{\Omega,\Delta}$  with  $\beta = 2$  (blue dash),  $\beta = 3$  (red thin solid), and  $\beta = 4$  (black solid) for the exciton model. b)  $Re\langle R_{1\beta}\rangle_{\Omega,\Delta}$  with  $\beta = 2$  (blue dash),  $\beta = 3$  (red thin solid), and  $\beta = 4$  (black solid) for the vibronic exciton model. c) Sum of all non-rephasing coherence pathways,  $\sum_{\alpha\beta} Re\langle R_{\alpha\beta}\rangle_{\Omega,\Delta}$ , giving rise to signal in the range  $12100 \pm 30 \text{ cm}^{-1}$  for the vibronic exciton model with  $v_0 = 185 \text{ cm}^{-1}$  (blue) and  $v_0 = 117 \text{ cm}^{-1}$  (red) at 77 K. The initial value of the signal is 0.48 and the first minimum at  $t_2 = 0.04 \text{ ps}$  has an amplitude of  $-0.23$ . The non-rephasing stimulated emission signal calculated for the same parameters and spectral range has an initial value of 0.17. d) Power spectrum of the Fourier transform of the signals in (c) starting from 0.2 ps.

oscillation frequency depends on transition energies, electronic couplings and vibrational frequencies according to Eq. (1). Figs. 2(c) and (d) compares the oscillations on the red edge of the spectrum for two different vibrational frequencies found in the FLN experiment,  $\omega_0 = 185 \text{ cm}^{-1}$  and  $\omega_0 = 117 \text{ cm}^{-1}$ . For  $\omega_0 = 117 \text{ cm}^{-1}$ , the oscillations have a frequency of  $140 \text{ cm}^{-1}$  and a shorter dephasing time as compared to  $\omega_0 = 185 \text{ cm}^{-1}$ . The dephasing time of the coherences depend on the amount of vibrational character of the vibronic exciton states, and detailed analysis of the oscillations provide information on the energies and nature of the eigenstates not accessible from linear spectra (see Fig. 1). However, the results in Figs. 2 (c) and (d) indicate that more than one vibrational mode needs to be included explicitly for a quantitative analysis of the oscillations in FMO.

In this work we have shown that the vibronic exciton model predicts coherences in FMO with 1.3 ps dephasing times at 77 K. Our model does not invoke static nor dynamic correlations in the site energies of the pigments, and uses experimentally determined spectral densities and vibrational frequencies. The long lived coherences are found to reflect coherent superpositions of vibronic exciton states with dominant contributions from vibra-

$\langle  c_{n,\nu}^\alpha ^2 \rangle_\Delta$	$\alpha = 1$	$\alpha = 2$	$\alpha = 3$	$\alpha = 4$
$n = 1, \nu = 0$	0.0	0.03	0.58	0.15
$n = 1, \nu = 1$	0.0	0.0	0.0	0.0
$n = 3, \nu = 0$	<b>0.75</b>	0.2	0.03	0.0
$n = 3, \nu = 1$	0.0	0.0	0.2	<b>0.67</b>
$n = 4, \nu = 0$	0.21	0.51	0.01	0.01
$n = 4, \nu = 1$	0.0	0.0	0.0	0.01
$\langle \mu_\alpha^2 \rangle_\Delta (\mu_{BChl}^2)$	<b>0.87</b>	0.58	1.3	<b>0.57</b>
$\langle E_\alpha \rangle_\Delta - \langle E_1 \rangle_\Delta (\text{cm}^{-1})$	0.0	105	175	217

Table I: Contributions of selected basis excitations ( $|c_{n,\nu}^\alpha|^2$ ) to the four first vibronic exciton states averaged over energetic disorder. The numbering of the pigments is defined in Fig. 1 and is the same as in Ref. [18]. The two bottom rows show the averaged transition strength in units of the BChl monomer, and the average energy differences between the vibronic exciton levels, respectively.

tional excitations on the same pigment. Because vibrational modes are an inherent property of all pigments, we expect vibronic excitons to be a general feature in the dynamics of molecular aggregates. In the exciton language, the long lived coherences reported here correspond to a coherence between the system and the bath. Because the resonance coupling in the vibronic exciton model acts on

the system as well as on certain bath modes (Eq. (1)), both types of DOF become mixed. This enhances the effective system-bath coupling in a way not accounted for in our exciton model. A similar mixing of system and bath DOF takes place implicitly when the reduced equation of motion for the electronic system is propagated exactly [16]. It is clear that the mixing takes place for all bath modes. However, modes of the protein environment are strongly damped and cannot contribute to a long dephasing time. As shown here, one or more of the underdamped vibrations found in the BChl monomers are needed to account for the enhanced dephasing times of the coherences. Our results imply that the oscillations in the 2D experiment on FMO reflect the dynamics of the nuclear DOF within a single pigment, which should have little impact on the transfer of energy from the chlorosome to the reaction centre.

*Acknowledgments:* This work was supported by the Wenner-Gren foundation, Österreichischer Austauschdienst (WTZ), Austrian Science Foundation (FWF), the Swedish Research Council, KAW foundation, Swedish Energy Agency, the Czech Science Foundation grant GACR 205/10/0989, and the Ministry of Education, Youth, and Sports of the Czech Republic, grant MEB 061107.

- 
- [1] A. S. Davydov, *Biology and Quantum Mechanics* (Pergamon Press, New York, 1981).
- [2] H. van Amerongen, L. Valkunas, and R. van Grondelle, *Photosynthetic Excitons* (World Scientific, Singapore, 2000).
- [3] O. Kühn, V. Sundström, and T. Pullerits, *Chem. Phys.* **275**, 15 (2002).
- [4] G. S. Engel, T. R. Calhoun, E. L. Read, T.-K. Ahn, T. Mančal, Y.-C. Cheng, R. E. Blankenship, and G. R. Fleming, *Nature* **446**, 782 (2007).
- [5] A. Ishizaki and G. R. Fleming, *Proc. Nat. Acad. Sci. USA* **106**, 17255 (2009).
- [6] D. Hayes, J. Wen, G. Panitchayangkoon, R. E. Blankenship, and G. S. Engel, *Faraday Discuss.* **150**, 459 (2011).
- [7] T. R. Calhoun, N. S. Ginsberg, G. S. Schlau-Cohen, Y.-C. Cheng, M. Ballottari, R. Bassi, and G. R. Fleming, *J. Phys. Chem. B* **113**, 16291 (2009).
- [8] E. Collini, C. Y. Wong, K. E. Wilk, P. M. G. Curmi, P. Brumer, and G. D. Scholes, *Nature* **463**, 644 (2010).
- [9] L. Chen, R. Zheng, Y. Jing, and Q. Shi, *J. Chem. Phys.* **134**, 194508 (2011).
- [10] B. Hein, C. Kreisbeck, T. Kramer, and M. Rodriguez, arXiv:1110.1511v2.
- [11] P. Nalbach, D. Braun, and M. Thorwart, *Phys. Rev. E* **84**, 041926 (2011).
- [12] D. Abramavicius and S. Mukamel, *J. Chem. Phys.* **134**, 174504 (2011).
- [13] F. Caycedo-Soler, A. W. Chin, J. Almeida, S. F. Huelga, and M. B. Plenio, arXiv:1201.0156v1.
- [14] C. Olbrich, J. Strumpfer, K. Schulten, and U. Kleinekathofer, *J. Phys. Chem. B* **115**, 758 (2011).
- [15] S. Shim, P. Rebentrost, S. Valleeau, and A. Aspuru-Guzik, arXiv:1104.2943v2.
- [16] G. Panitchayangkoon, D. Voronine, D. Abramavicius, J. R. Caram, N. H. C. Lewis, S. Mukamel, and G. S. Engel, *Proc. Nat. Acad. Sci. USA* **108**, 20908 (2011).
- [17] V. May and O. Kühn, *Charge and Energy Transfer Dynamics in Molecular Systems* (Wiley-VCH, Berlin, 2001).
- [18] J. Adolphs and T. Renger, *Biophys. J.* **91**, 2778 (2006).
- [19] N. Christensson, F. Milota, J. Hauer, J. Sperling, O. Bixner, A. Nemeth, and H. Kauffmann, *J. Phys. Chem. B* **115**, 5383 (2011).
- [20] M. Wendling, T. Pullerits, M. A. Przyjalowski, S. I. E. Vulto, T. J. Aartsma, R. van Grondelle, and H. van Amerongen, *J. Phys. Chem. B* **104**, 5825 (2000).
- [21] S. Polyutov, O. Kuhn, and T. Pullerits, *Chem. Phys.* **394**, 21 (2012).
- [22] M. R. Philpott, *J. Chem. Phys.* **55**, 2039 (1971).
- [23] F. C. Spano, *J. Chem. Phys.* **116**, 5877 (2002).
- [24] S. Mukamel, *Principles of nonlinear optical spectroscopy* (Oxford University Press, Oxford, 1995).
- [25] W. M. Zhang, T. Meier, V. Chernyak, and S. Mukamel, *J. Chem. Phys.* **108**, 7763 (1998).
- [26] D. E. Tronrud, J. Wen, L. Gay, and R. Blankenship, *Photosynth. Res.* **100**, 79 (2009).
- [27] W. Humphrey, A. Dalke, and K. Schulten, *J. Mol. Graphics* **14**, 33 (1996).